

Investigation of Interfacial Tensions for Carbon Dioxide Aqueous Solutions by Perturbed-Chain Statistical Associating Fluid Theory Combined with Density-Gradient Theory

Xiao-Sen Li,[†] Jian-Min Liu,[‡] and Dong Fu^{*,‡}

Key Laboratory of Renewable Energy and Gas Hydrate, Guangzhou Institute of Energy Conversion, Chinese Academy of Sciences, Guangzhou, 510640, People's Republic of China and School of Environmental Science and Engineering, North China Electric Power University, Baoding, 071003, People's Republic of China

The perturbed-chain statistical associating fluid theory and density-gradient theory are used to construct an equation of state (EOS) applicable for the phase behaviors of carbon dioxide aqueous solutions. With the molecular parameters and influence parameters respectively regressed from bulk properties and surface tensions of pure fluids as input, both the bulk and interfacial properties of carbon dioxide aqueous solutions are satisfactorily correlated by adjusting the binary interaction parameter (k_{ij}). Our results show that the constructed EOS is able to describe the interfacial properties of carbon dioxide aqueous solutions in a wide temperature range, and illustrate the influences of temperature, pressure, and densities in each phase on the interfacial properties.

1. Introduction

Supercritical carbon dioxide (SC-CO₂) is an inexpensive, nonflammable, nontoxic, and environmentally benign solvent with many special properties. Its density, compressibility, solvent power and dielectric constant can be tuned over a wide range by changing the pressure or temperature, which is of great interest not only from a fundamental point of view but also for industrial processes. The behavior of SC-CO₂ mixtures has been a subject of considerable interest. For example, the phase behaviors of CO₂-hydrocarbon mixtures^{1–16} have been extensively investigated because the data for solubility of both CO₂ in hydrocarbons and hydrocarbons in CO₂ are very important. Besides the behaviors of CO₂-hydrocarbon mixtures, the behaviors of CO₂-water mixtures^{17–33} are also very important in many industrial processes like water extraction and CO₂ sequestration. As SC-CO₂ and water are solvents with very low mutual solubilities, SC-CO₂ is a promising candidate as a solvent for water extraction processes. Moreover, injecting carbon dioxide into saline aquifers, abandoned hydrocarbon reservoirs, unminable coal seams, or oceans becomes an interesting issue for CO₂ sequestration. In both of the water extraction and CO₂ sequestration processes, the interfacial tensions of CO₂-water mixtures are of fundamental interest because they play an important role in mass transfer limitations, mass transfer area, wetting behavior and formation of microemulsions or nucleus of hydrates.

In recent years, there was some research concerning the measurements of the interfacial tensions of CO₂-water mixtures. Chum and Wilkinson³¹ measured the interfacial tensions of CO₂-water mixtures at temperatures ranging from 278.15 to 344.15 K and pressures ranging from 0.1 to 18.6 MPa with a capillary rise method. Tewel and co-workers³² investigated the thermodynamic and dynamic interfacial properties of CO₂-water mixtures and analyzed the mechanisms that influence the interfacial tensions. Very recently, Kvamme and co-

workers³³ developed a novel apparatus and measured the interfacial tensions of CO₂-water mixtures at temperatures ranging from 278.15 to 335.15 K and pressures ranging from 0.1 to 20 MPa. However, the theoretical studies on the interfacial properties like interfacial tensions and density distributions of CO₂ and water have rarely been reported so far.

The main purpose of this work is to develop an approach that can well describe both the bulk and interfacial properties of CO₂-water mixtures and then demonstrate how the temperature, pressure, and density in each phase affects the interfacial properties. To this end, we apply the widely used perturbed-chain statistical associating fluid theory (PC-SAFT)^{13,14,34–49} to formulate the uniform equation of state, and then extend it to the interface by combining the density gradient theory (DGT).^{48–67} With the molecular parameters and influence parameters of pure fluids as input, the interfacial tensions of CO₂-water mixtures in the temperature range 278.15–344.15 K are investigated.

2. Theory

For a binary mixture with two equilibrium phases separated by an interface, the Helmholtz free energy density $f[\rho_1(\mathbf{r}), \rho_2(\mathbf{r})]$ could be described through expansion in a Taylor series.^{48–67} The expansion is expressed as follows:

$$f[\rho_1(\mathbf{r}), \rho_2(\mathbf{r})] = f_0[\rho_1(\mathbf{r}), \rho_2(\mathbf{r})] + \sum_{ij} \frac{1}{2} \kappa_{ij} \nabla \rho_i(\mathbf{r}) \nabla \rho_j(\mathbf{r}) + \dots \quad (1)$$

where $\rho_i(\mathbf{r})$ is the local number density of molecule i at position \mathbf{r} and $\nabla[\rho_i(\mathbf{r})]$ is the corresponding local density gradient. $f_0[\rho_1(\mathbf{r}), \rho_2(\mathbf{r})]$ is the free energy density for the bulk phase. κ_{11} , κ_{22} are, respectively, the influence parameters for components 1 and 2, and $\kappa_{12} = \sqrt{\kappa_{11}\kappa_{22}}$ is the cross-influence parameter.

Keeping the lowest order term in the expansion, the Helmholtz free energy can be expressed as follows:

$$A[\rho_1(\mathbf{r}), \rho_2(\mathbf{r})] = \int \left[f_0[\rho_1(\mathbf{r}), \rho_2(\mathbf{r})] + \sum_{ij} \frac{1}{2} \kappa_{ij} \nabla \rho_i(\mathbf{r}) \nabla \rho_j(\mathbf{r}) \right] d\mathbf{r} \quad (2)$$

* To whom correspondence should be addressed. X. S. Li, E-mail: lixs@ms.giec.ac.cn Tel. 86-20-80757037; D. Fu, E-mail: fudong@tsinghua.org.cn. Tel. 86-312-7523127.

[†] Chinese Academy of Sciences.

[‡] North China Electric Power University.

In equilibrium state, the density profiles across the interface must satisfy the following Euler–Lagrange equation:

$$\sum_j \nabla [\kappa_{ij} \nabla \rho_j(\mathbf{r})] - \frac{1}{2} \sum_k \sum_j \frac{\partial \kappa_{kj}}{\partial \rho_i(\mathbf{r})} \nabla \rho_k(\mathbf{r}) \nabla \rho_j(\mathbf{r}) = \frac{\partial \Omega[\rho_1(\mathbf{r}), \rho_2(\mathbf{r})]}{\partial \rho_i(\mathbf{r})} \quad (3)$$

where the grand potential density $\Omega[\rho_1(\mathbf{r}), \rho_2(\mathbf{r})] = f[\rho_1(\mathbf{r}), \rho_2(\mathbf{r})] - \sum_i \mu_i^0 \rho_i(\mathbf{r})$ and $\mu_i^0 = \partial \{f_0[\rho_1(\mathbf{r}), \rho_2(\mathbf{r})]\} / \partial \rho_i(\mathbf{r})|_{T, V, \rho_j(\mathbf{r})}$ is the chemical potential of component i of bulk phase.

Because the density varies only in the direction perpendicular to the interface (z direction), $\rho(\mathbf{r})$ can be replaced by $\rho(z)$. eq 3 is then rewritten as follows:

$$\sum_j \frac{\partial}{\partial z} \left[\kappa_{ij} \frac{\partial \rho_j(z)}{\partial z} \right] - \frac{1}{2} \sum_k \sum_j \frac{\partial \kappa_{kj}}{\partial \rho_i(z)} \frac{\partial \rho_k(z)}{\partial z} \frac{\partial \rho_j(z)}{\partial z} = \frac{\partial \Omega[\rho_1(z), \rho_2(z)]}{\partial \rho_i(z)} \quad (4)$$

Assuming that the density-dependence of the influence parameters can be neglected, eq 4 becomes:

$$\sum_j \kappa_{ij} \frac{d^2 \rho_j(z)}{dz^2} = \mu_i[\rho_1(z), \rho_2(z)] - \mu_i^0 \quad (5)$$

where $\mu_i[\rho_1(z), \rho_2(z)]$ is the chemical potential of component i in the interface.

Multiplying eq 5 by $d\rho_i(z)/dz$, summing over i and integrating, we obtain:

$$\sum_i \sum_j \frac{1}{2} \kappa_{ij} \frac{d\rho_i(z)}{dz} \frac{d^2 \rho_j(z)}{dz^2} = \Omega[\rho_1(z), \rho_2(z)] + p^{\text{coex}} = \Delta\Omega[\rho_1(z), \rho_2(z)] \quad (6)$$

where μ_i^0 and p^{coex} are, respectively, the chemical potential of component i and the saturated pressure in the bulk phase.

During the determination of density profiles $\rho_1(z)$ and $\rho_2(z)$, one should first select a reference fluid. For example, when component 2 is selected as the reference fluid, the density gradient of the reference fluid is expressed as follows:

$$\frac{d\rho_2(z)}{dz} = \sqrt{\frac{\Delta\Omega[\rho_1(z), \rho_2(z)]}{\kappa}} \quad (7)$$

where κ is the influence parameter for binary mixture, which can be formulated as follows:

$$\kappa = \kappa_{11} \left[\frac{d\rho_1(z)}{d\rho_2(z)} \right]^2 + 2\kappa_{12} \frac{d\rho_1(z)}{d\rho_2(z)} + \kappa_{22} \quad (8)$$

Dividing the vapor–liquid surface into N_0 thin layers, the number density in the k th layer can be expressed as follows:

$$\rho_2(z_k) = \rho_2(z_{k-1}) + \Delta\rho_2 \quad (9)$$

where $\rho_2(z_0)$ and $\rho_2(z_{N_0+1})$ are respectively equal to the equilibrium vapor density ρ_2^V and the equilibrium liquid density ρ_2^L . $\Delta\rho_2$ is defined as follows:

$$\Delta\rho_2 = (\rho_2^L - \rho_2^V) / N_0 \quad (10)$$

The number density of component 1 in the k th layer is as follows:

$$\rho_1(z_k) = \rho_1(z_{k-1}) + \frac{d\rho_1(z_{k-1})}{d\rho_2(z_{k-1})} \Delta\rho_2, \text{ with } \rho_1(z_0) = \rho_1^V, \rho_1(z_{N_0+1}) = \rho_1^L \quad (11)$$

Table 1. Molecular Parameters and Influence Parameters

	m	$\sigma/10^{-10}\text{m}$	$\epsilon/k^{-1}/\text{K}$	$\kappa^a \times 100$	$\epsilon^a/k^{-1}/\text{K}$	$\kappa/10^{-19}\text{J}\cdot\text{m}^5\cdot\text{mol}^{-2}$
water	1.057	2.936	366.55	3.8500	2500.7	0.062
CO ₂	2.073	2.785	169.21			0.140

where the differentiation $d\rho_1/d\rho_2$ in $(k-1)$ th layer is expressed as follows:

$$\frac{d\rho_1}{d\rho_2} = \frac{\sqrt{\kappa_{22}[\partial\mu_1/\partial\rho_2]_{T,p,\rho_1}} - \sqrt{\kappa_{11}[\partial\mu_1/\partial\rho_2]_{T,p,\rho_1}}}{\sqrt{\kappa_{11}[\partial\mu_2/\partial\rho_1]_{T,p,\rho_2}} - \sqrt{\kappa_{22}[\partial\mu_1/\partial\rho_1]_{T,p,\rho_2}}} \quad (12)$$

where μ_1 and μ_2 are the chemical potentials for components 1 and 2, respectively.

Suppose ρ_2^V corresponds to $z = 0$, the value of z in each layer can be calculated from:

$$z = \int_{\rho_2^V}^{\rho_2} \sqrt{\frac{\kappa}{\Delta\Omega[\rho_1, \rho_2]}} d\rho_2 \quad (13)$$

By evaluating the integral numerically, a distance z may be determined for any ρ_2 lying between the bulk densities, hence $\rho_1(z)$ and $\rho_2(z)$ can be determined. The theoretical details of DGT can be found in the work of Miqueu and co-workers.^{65,66}

Once the equilibrium density profiles are obtained, the surface tension can be calculated from:

$$\gamma = 2 \int_{\rho_2^V}^{\rho_2^L} \sqrt{\Delta f[\rho_1, \rho_2]} \kappa d\rho_2 \quad (14)$$

3. Results and Discussion

In this work, the Helmholtz free energy, A , for binary mixtures is expressed by PC-SAFT. The details of the formulations can be found in the work of Gross and Sadowski.^{34,35}

At given temperature, T , the vapor–liquid equilibria of CO₂–water mixtures can be determined according to the requirement:

$$\begin{cases} p^I = p^{II} \\ \mu_1^I = \mu_1^{II}, \mu_2^I = \mu_2^{II} \end{cases} \quad (15)$$

where I and II stand for upper and lower phases of the mixtures, respectively. The variable p is the pressure, $\mu_1 = \langle \partial[A(\rho_1 + \rho_2)] / \partial \rho_1 \rangle_{T, V, \rho_2}$ and $\mu_2 = \langle \partial[A(\rho_1 + \rho_2)] / \partial \rho_2 \rangle_{T, V, \rho_1}$ are the chemical potentials for CO₂ and water, respectively. Using the analytical expression of Helmholtz free energy A given by Gross and Sadowski,^{34,35} μ_1 and μ_2 can be obtained by numerical differentiation.

In the calculations of vapor–liquid equilibria, there are three molecular parameters for CO₂: segment number, m ; soft sphere diameter of each segment, σ ; and dispersion energy parameter of each segment, ϵ/k . For water, there are two additional parameters: association volume, κ^a , and association energy, ϵ^a/k . Following the work of Gross and Sadowski,³⁵ there are two association sites on each molecule. The molecular parameters of CO₂ are directly taken from the work of Gross and Sadowski³⁴ but those of water are regressed by fitting to the experimental data of vapor pressure and liquid densities, as listed in Table 1. It is worth noting that in the work of Gross and Sadowski,³⁵ the molecular parameters of water have been well regressed with a minimum average relative deviation for saturated pressure and liquid density, but the liquid densities at low temperatures are significantly underestimated. Compared with the molecular parameters present in the work of Gross and Sadowski,³⁵ those listed in Table 1 yield very close average

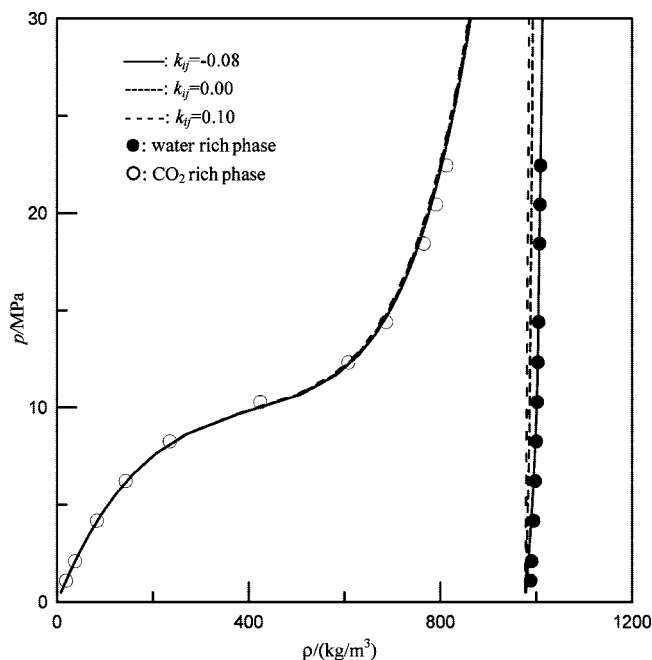


Figure 1. The influence of k_{ij} on the vapor–liquid equilibria of CO₂–water binary mixtures. $T = 323.15$ K. Lines: from PC-SAFT. Symbols: experimental data.³³

relative deviations but reproduce the liquid densities more accurately at low temperatures.

3.1. Equilibrium Densities in Bulk Phases. Figure 1 shows the comparison of the experimental and calculated vapor–liquid equilibria for CO₂–water binary mixtures at $T = 323.15$ K. We find from the calculations that the change of binary interaction parameter (k_{ij}) actually have little effect on the densities in the CO₂-rich phase but have distinguishable effect on the densities in water-rich phase. It is worth noting that there are some experimental data of the equilibrium phase compositions for CO₂–water mixtures, but we find they are very difficult to accurately correlate. Moreover, we find that PC-SAFT cannot simultaneously describe the phase equilibria and interfacial tensions of CO₂–water mixtures in a wide temperature range using a single binary interaction parameter, k_{ij} . As the main purpose of this work is to illustrate the influences of temperature, pressure, and density in each phase on the interfacial properties, we use the experimental data of bulk densities (298.15–323.15 K) and the interfacial tensions (278.15–344.15 K) to fit k_{ij} and express it as a function of temperature. The temperature dependent k_{ij} is regressed as follows:

$$k_{ij} = 7.461 \times 10^{-4}T - 0.201 \quad (16)$$

Using eq 16, vapor–liquid equilibria for CO₂–water binary mixtures at different temperatures can be determined. Figure 2 shows the results under the temperatures from 288.15 to 344.15 K. From this figure, one finds that the CO₂-rich phase presents different behaviors at different temperatures and pressures. At 288.15, 298.15, and 303.15 K, there are obvious jumps in the density–pressure curves, and the pressure at which the jump occurs increases with increasing temperature. However, in the cases of higher temperatures, the jump disappears. At very low pressures, the mass densities at different temperatures are very close and all are of small values, however, when the pressures get higher, the mass densities decrease rapidly with increasing temperature. Compared with the CO₂-rich phase, the water-rich phase presents simpler behaviors. The mass density decreases

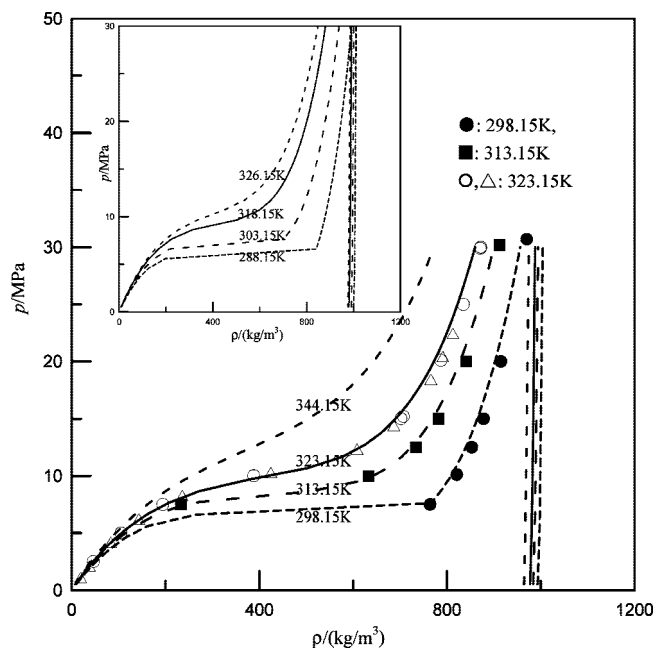


Figure 2. Vapor–liquid equilibria for CO₂–water binary mixtures from 288.15 to 344.15 K. Lines: predicted from PC-SAFT, with the k_{ij} values expressed by eq 16. Symbols: experimental data.^{18,33}

observably with increasing temperature at a given pressure, and increases slightly with increasing pressure at a given temperature.

3.2. Density Distributions Across the Interface. Results of the equilibrium bulk properties can be used to derive information about the structure and properties of the interface between coexisting phases. To obtain the interfacial properties, one should first determine the influence parameters for each pure component. In this work, the influence parameters for water and CO₂ are regressed by fitting their surface tensions to the experimental data,^{68–70} as also shown in Table 1. Using the bulk properties and the influence parameters of pure component as input, one can calculate the equilibrium density profiles across the interface by numerically evaluating eq 13.

In the numerical calculations, care must be taken in the selection of a reference fluid. The density profile of the reference fluid must be a monotonic function of z over the whole interface. In this work, we select water (component 2) as the reference fluid. Once the reference fluid is selected, we first set $\Delta\rho_2$ as $(\rho_2^L - \rho_2^V)/10\,000$ (N_0 should be no less than 10 000, otherwise the interfacial tensions cannot be fully convergent) and then use eq 9 to define the number densities of water, $\rho_2(z_i, i = 1 \dots N_0)$.

The determination of each $\rho_1(z_i)$ is complex. One first needs to solve the numerical differentiations for $[\partial\mu_1/\partial\rho_2]_{T,p,\rho_1}$, $[\partial\mu_1/\partial\rho_2]_{T,p,\rho_1}$, $[\partial\mu_2/\partial\rho_1]_{T,p,\rho_2}$, and $[\partial\mu_1/\partial\rho_1]_{T,p,\rho_2}$ to obtain $[d\rho_1/d\rho_2]_{i-1}$, and then substitute $[d\rho_1/d\rho_2]_{i-1}$ into eq 11 to obtain $\rho_1(z_i)$. When both $\rho_1(z_i)$ and $\rho_2(z_i)$ are available, the influence parameter of binary mixture κ and the excess grand potential density $\Delta\Omega[\rho_1(z_i), \rho_2(z_i)]$ can be calculated, respectively, using eqs 8 and 6. Suppose ρ_2^V corresponds to $z = 0$, z_i corresponding to $\rho_1(z_i)$ and $\rho_2(z_i)$ can be determined using eq 13. Repeating the above-mentioned process $N_0 - 1$ times, one can obtain the density profiles $\rho_1(z)$ and $\rho_2(z)$.

Figure 3, parts a and b, shows the density distributions of CO₂ and water across the interface and the influences of temperature and pressure. In both parts a and b, the density profiles of CO₂ display a nonmonotonic trend at the interface, indicating that the molecules of CO₂ accumulate in the interface. Actually, for a binary mixture, if the components have two quite

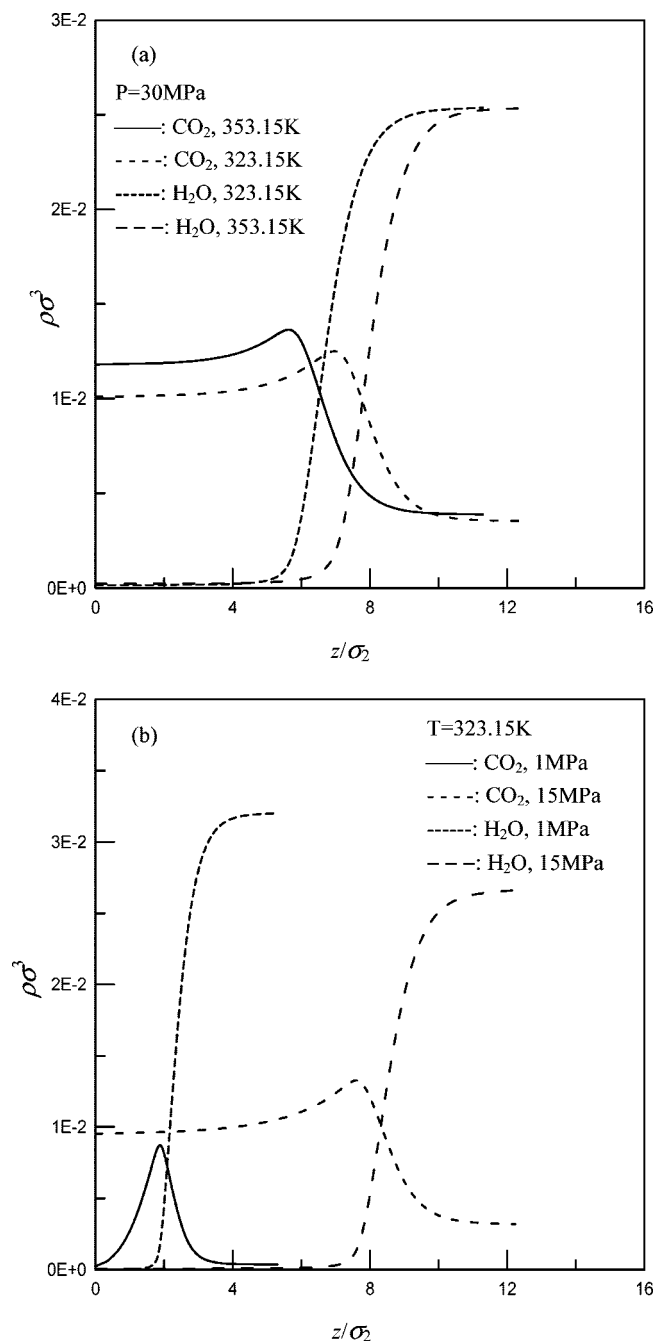


Figure 3. Influences of pressure (a) and temperature (b) on the density distributions of CO₂ and water across the interface. Lines: predicted from PC-SAFT+DGT. Component 2, water is the reference fluid.

different molecules, molecules of the component with lowest surface tension have a tendency to accumulate in the interface. Figure 3(a) indicates that when the pressure is high (30 MPa), the reduced number densities of CO₂ in CO₂-rich phases remarkably decrease with increasing temperature but those in water-rich phases decrease indistinctively. The reduced number densities of water in both CO₂-rich and water-rich phases indistinctively decrease with increasing temperature. This may explain why the mass densities of the CO₂-rich phase significantly decrease with the increase of temperature at high pressure, yet those of water-rich phase indistinctively decrease (see Figure 2). From Figure 3(b), one finds the pressure also remarkably affects the density distributions. At a given temperature, with increasing pressure, the reduced number densities of CO₂ in both CO₂-rich and water-rich phases increase remarkably.

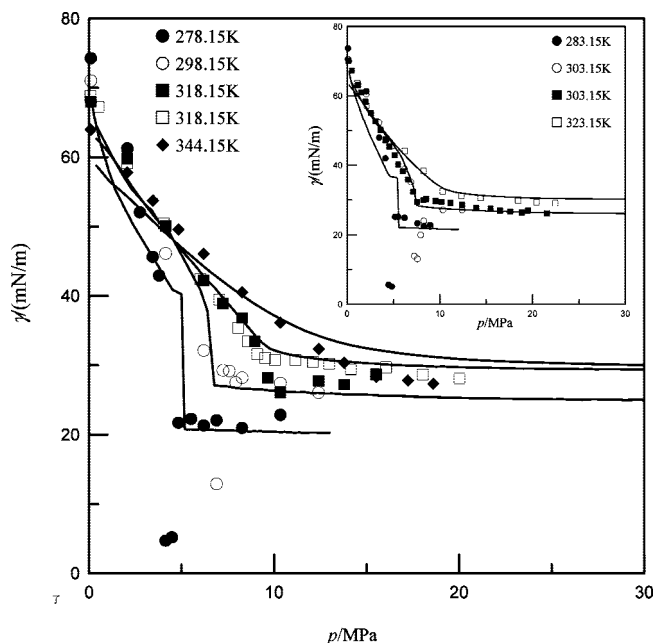


Figure 4. The pressure and temperature dependencies of surface tensions. In the main plot, $T = 278.15, 298.15, 318.15,$ and 344.15 K; in the insert plot, $T = 283.15, 303.15,$ and 323.15 K. Symbols: experimental data^{31,33} Lines: from PC-SAFT+DGT.

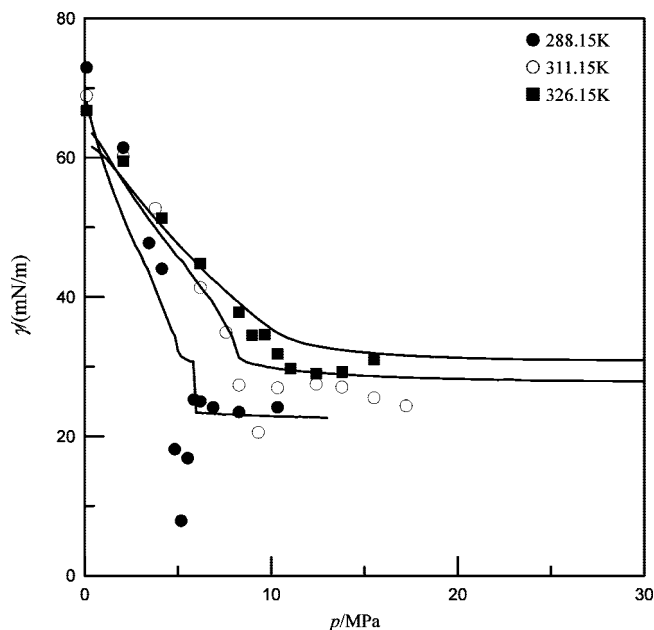


Figure 5. The pressure and temperature dependencies of surface tensions at 288.15, 311.15, and 326.15 K. Symbols: experimental data^{31,33} Lines: from PC-SAFT+DGT.

However, those of water decrease remarkably in the water-rich phase, yet indistinctively in CO₂-rich phase. In the CO₂-rich phase, as the number densities of CO₂ and water respectively remarkably increase and indistinctively decrease, the total number densities increase rapidly, leading to the strong pressure dependence of the mass density in CO₂-rich phase. In the water-rich phase, because the increase of CO₂ density remedies the decrease of water density, the mass density increases slightly (see Figure 2).

3.3. Interfacial Tensions. Figures 4 and 5 show the pressure and temperature dependencies of interfacial tensions from 278.15 to 344.15 K. One finds from the experimental data that below the critical temperature of CO₂ (304 K), each interfacial tension

isotherm is interrupted at the vapor–liquid coexistence line of CO₂ phase and presents a jump at a certain pressure. The isotherm respectively reflects the interfacial tension of water with gaseous CO₂, and water with liquid CO₂ below and above this pressure. The interfacial tensions decrease nearly linearly with pressure before the jumps yet decrease very slightly after the jumps. Above the critical temperature of CO₂, as the VLL three-phase point disappears, the jumps disappear in both the density–pressure curves and the interfacial tension isotherms. Along all of the investigated temperature range, with the increase of temperature, the interfacial tensions decrease at low pressures but increase at high pressures. One also finds that there are some cusps in the experimental interfacial tension isotherms at low temperatures (278.15–311.15 K), but Kvamme and co-workers³³ confirmed that this phenomenon can be avoided by improving the experimental methods.

The theoretical model well captures the temperature dependence. As shown in Figures 4 and 5, at very low pressures, the interfacial tension decreases with the increase of temperature, yet the opposite effect is found at higher pressures. This phenomenon can be explained by the equilibrium densities in bulk phases. At very low pressures, the CO₂ densities at different temperatures are of very small values, the interfacial tensions of the mixtures should be close to those of pure water. Taking into account that the surface tension of pure water decreases with the decrease of the liquid density, the lower interfacial tension for the mixture of CO₂ and water with lower density is reasonable, hence the interfacial tension of the mixtures decreases with the increase of temperature. At relatively higher pressures, the CO₂ density decreases very rapidly with the increase of temperature (see Figure 2, the higher the temperature, the lower the CO₂ density becomes), which makes the interfacial tensions decrease very rapidly.

The theoretical model also well captures the pressure dependence. For example, in the case of $T = 278.15$ K, a jump occurs at the pressure $p = 4.99$ MPa. Around this pressure, the interfacial tension abruptly decreases from 40.25 to 20.83 mN/m. When the pressure is higher than 5.16 MPa, all of the predicted interfacial tensions are very close to 20.83 mN/m. Similar behaviors can be found in the cases of $T = 283.15$, 288.15, 298.15, and 303.15 K, despite that the corresponding jumps occur respectively at pressures $p = 5.42$, 5.81, 6.39, and 7.14 MPa, and the scopes of the jumps get narrower with the increase of temperature. We have verified that when the temperature is higher than 307.7 K (the experimental one is $T = 304$ K³³), the interfacial tensions decrease monotonously with the pressure and there are no jumps in all isotherms.

The impressive pressure dependence of interfacial tensions may be explained by the pressure dependence of bulk properties shown in Figure 2. Actually, in the framework of DGT, the equilibrium densities in the bulk phases play very important roles in the calculations of interfacial properties. As in the investigated temperature range, the interfacial tension of CO₂ is smaller than that of water, the rapid increase of CO₂ density (see Figure 2) makes the interfacial tensions of mixtures decrease rapidly. In the plateau of density–pressure curve, the extremely rapid increase of CO₂ density yields a jump in the interfacial tension isotherm. When the pressures are high, both densities in CO₂-rich phase and water-rich phase increase very slightly, hence the interfacial tensions of the mixtures tend to remain a constant.

4. Conclusions

The bulk and interfacial properties of CO₂–water binary mixtures are investigated by using the PC-SAFT and DGT. The influences of temperature, pressure, and equilibrium densities on the interfacial properties are demonstrated. The results show the following:

(1) PC-SAFT is able to accurately reproduce the densities in CO₂-rich and water-rich phases and satisfactorily describe the temperature and pressure dependence of densities in both phases. At low temperatures, the jumps in the density–pressure curves of CO₂ can be well predicted and the pressure at which the jump occurs increases with the increase of temperature. However, when the temperature is higher than 307.7 K, the predicted density of CO₂-rich phase increases monotonously with the pressure.

(2) By combining DGT, PC-SAFT is able to correlate and predict the interfacial tensions for CO₂–water binary mixtures. In the investigated temperature range, with the increase of temperature, the interfacial tensions decrease at low pressures but increase at high pressures. At low temperatures, PC-SAFT+DGT predicts jumps in the interfacial tension isotherms. The interfacial tensions decrease nearly linearly with pressure before the jumps yet decrease very slightly after the jumps. The temperature and pressure dependences of interfacial tensions as well as the jumps in the interfacial tension isotherms can be well predicted compared with experimental data. When the temperature is higher than 307.7 K, the interfacial tensions predicted by PC-SAFT+DGT decrease monotonously with the pressure, without any jumps in the interfacial tension isotherms.

List of symbols

A , Helmholtz free energy, J;
 f , Helmholtz free energy density, $\text{J}\cdot\text{m}^{-3}$;
 k_{ij} , binary interaction parameter;
 k , Boltzmann constant, $\text{J}\cdot\text{K}^{-1}$;
 m , number of segment;
 N_0 , total number of thin layers for the vapor–liquid surface;
 p , pressure, Pa;
 T , absolute temperature, K;
 x , mole fraction.
Greek Letters. β , $1/kT$;
 γ , surface tension, $\text{mN}\cdot\text{m}^{-1}$;
 ε , dispersion energy parameter for each segment, J;
 ε^a , association energy parameter, J;
 κ , influence parameter, $\text{J}\cdot\text{m}^5\cdot\text{mol}^{-2}$;
 κ^a , measure of association volume;
 μ , chemical potential, $\text{J}\cdot\text{mol}^{-1}$;
 ρ , number density of molecules, m^{-3} ;
 mass density, $\text{kg}\cdot\text{m}^{-3}$;
 σ , hard core diameter for each segment, 10^{-10}m ;
 Ω , grand potential density, $\text{J}\cdot\text{m}^{-3}$;
Superscripts. I , II , upper and lower phases;
Subscripts. i , j , components;

Acknowledgment

The authors appreciate financial support from the National High Technology Research and Development Program of China (No. 2006AA05Z319). D.F. is grateful for financial support from the National Natural Science Foundation of China (No. 20606009), the Program for New Century Excellent Talents in University (No. 06-0206), the key program from NCEPU and

the Research Fund of Key Laboratory for Nanomaterials, Ministry of Education (No.2006-2).

Literature Cited

- (1) Turek, E. A.; Metcalfe, R. S.; Fishback, R. E. Phase behavior of several carbon dioxide/west-Texas-reservoir-oil systems. *SPE Reservoir Eng.* **1988**, *3*, 505–516.
- (2) Levelt Sengers, J. M. H. *Supercritical Fluids: Their Properties and Applications*; Kiran, E., Debenedetti, P. G., Peters, C. J., Eds.; Kluwer Academic Publishers: Dordrecht, 2000; Vol. 366.
- (3) Jofe, J.; Zudkevitch, D. Fugacity coefficients in gas mixtures containing light hydrocarbons and carbon dioxide. *Ind. Eng. Chem. Fund.* **1966**, *5*, 455–462.
- (4) Myers, A. L.; Prausnitz, J. M. Thermodynamics of solid carbon dioxide solubility in liquid solvents at low temperatures. *Ind. Eng. Chem. Fund.* **1965**, *4*, 209–212.
- (5) Vradman, L.; Herskowitz, M.; Korin, E.; Wisniak, J. Regeneration of poisoned nickel catalyst by supercritical CO₂ extraction. *Ind. Eng. Chem. Res.* **2001**, *40*, 1589–1590.
- (6) Bordet, F.; Passarello, J. P.; Chartier, T.; Tufeu, R.; Baumard, J. F. Modeling solutions of hydrocarbons in dense CO₂ gas. *J. Eur. Ceram. Soc.* **2001**, *21*, 1219–1227.
- (7) Nung, W. C.; Tsai, F. N. Correlation of vapor–liquid equilibrium for systems of carbon dioxide + hydrocarbon by the corresponding-states principle. *Chem. Eng. J.* **1997**, *66*, 217–221.
- (8) Kato, H.; Nagahama, K.; Hirata, M. Generalized interaction parameters for the Peng–Robinson equation of state: carbon dioxide-*n*-paraffin binary systems. *Fluid Phase Equilib.* **1981**, *4*, 219–231.
- (9) Kordas, K.; Tsoutsouras, K.; Stamatakis, S.; Tassios, D. A. generalized correlation for the interaction coefficients of CO₂–hydrocarbon binary mixtures. *Fluid Phase Equilib.* **1994**, *93*, 141–166.
- (10) Trebble, M. A.; Salim, P. H.; Sigmund, P. M. A generalized approach to prediction of two and three phase CO₂–hydrocarbon equilibria. *Fluid Phase Equilib.* **1993**, *82*, 111–118.
- (11) Passarello, J. P.; Benzaghoul, S.; Tobaly, P. Modeling mutual solubility of *n*-alkanes and CO₂ using SAFT equation of state. *Ind. Eng. Chem. Res.* **2000**, *39*, 2578.
- (12) Polishuk, I.; Wisniak, J.; Segura, H. Simultaneous prediction of the critical and sub-critical phase behavior in mixtures using equations of state II. Carbon dioxide-heavy *n*-alkanes. *Chem. Eng. Sci.* **2003**, *58*, 2529–2550.
- (13) García, J.; Lugo, L.; Fernández, J. Phase equilibria, PVT behavior, and critical phenomena in carbon dioxide+*n*-alkane mixtures using the perturbed-chain statistical associating fluid theory approach. *Ind. Eng. Chem. Res.* **2004**, *43*, 8345–8353.
- (14) Fu, D.; Liang, L. L.; Li, X.-S.; Yan, S. M.; Liao, T. Investigation of vapor–liquid equilibria for supercritical carbon dioxide and hydrocarbon mixtures by perturbed-chain statistical associating fluid theory. *Ind. Eng. Chem. Res.* **2006**, *45*, 4364–4370.
- (15) Mejía, A.; Polishuk, I.; Segura, H.; Wisniak, J. Estimation of interfacial behavior using the global phase diagram approach: I. Carbon dioxide–*n*-alkanes. *Thermochim. Acta* **2004**, *411*, 171–176.
- (16) Enders, S.; Kahl, H.; Winkelmann, J. Interfacial properties of polystyrene in contact with carbon dioxide. *Fluid Phase Equilib.* **2005**, *228–229*, 511–522.
- (17) Sako, T.; Sugeta, T.; Nakazawa, N.; Obuko, T.; Sato, M.; Taguchi, T.; Hiaki, T. Phase equilibrium study of extraction and concentration of furfural produced in reactor using supercritical carbon dioxide. *J. Chem. Eng. Jpn.* **1991**, *24*, 449–454.
- (18) Zappe, J.; Wesch, A.; Ebert, K. H. Measurement of the mass transfer into single drops in the system of water/supercritical carbon dioxide. *J. Colloid Interface Sci.* **2000**, *231*, 1–7.
- (19) King, M. B.; Mubarak, A.; Kim, J. D.; Bott, T. R. The mutual solubilities of water with supercritical and liquid carbon dioxide. *J. Supercrit. Fluids* **1992**, *5*, 296–302.
- (20) Bamberger, A.; Sieder, G.; Maurer, G. High-pressure (vapor–liquid) equilibrium in binary mixtures of (carbon dioxide - water or acetic acid) at temperatures from 313 to 353 K. *J. Supercrit. Fluids* **2000**, *17*, 97–100.
- (21) Li, X. S.; Englezos, P. Vapor–liquid equilibrium of systems containing alcohols, water, carbon dioxide and hydrocarbons using SAFT. *Fluid Phase Equilib.* **2004**, *224*, 111–118.
- (22) Carroll, J. J.; Mather, A. E. The system carbon dioxide–water and the Krichevsky–Kasarnovsky equation. *J. Solution Chem.* **1992**, *21*, 607–621.
- (23) Coan, C. R.; King, A. D., Jr. Solubility of water in compressed carbon dioxide, nitrous oxide, and ethane. Evidence for hydration of carbon dioxide and nitrous oxide in the gas phase. *J. Am. Chem. Soc.* **1971**, *93*, 1857–1862.
- (24) Crovetto, R. Evaluation of solubility data for the system CO₂–H₂O from 273 K to the critical point of water. *J. Phys. Chem. Ref. Data* **1991**, *20*, 575–589.
- (25) Kerrick, D. M.; Jacobs, G. K. A modified Redlich–Kwong equation for H₂O, CO₂ and H₂O–CO₂ mixtures at elevated pressures and temperatures. *Am. J. Sci.* **1981**, *281*, 735–767.
- (26) Anderson, G. K. Solubility of carbon dioxide in water under incipient clathrate formation conditions. *J. Chem. Eng. Data* **2002**, *47*, 219–222.
- (27) Seo, Y. T.; Lee, H.; Yoon, J. H. Hydrate phase equilibria of the carbon dioxide, methane, and water system. *J. Chem. Eng. Data* **2001**, *46*, 381–384.
- (28) Shyu, G.-S.; Hanif, N. S. M.; Hall, K. R.; Eubank, P. T. Carbon dioxide–water phase equilibria results from the Wong–Sandler combining rules. *Fluid Phase Equilib.* **1997**, *130*, 73–85.
- (29) Teng, H.; Yamasaki, A.; Chun, M.-K.; Lee, H. Solubility of liquid CO₂ in water at temperatures from 278 to 293 K and pressures from 6.44 to 29.49 MPa and densities of the corresponding aqueous solutions. *J. Chem. Thermodyn.* **1997**, *29*, 1301–1310.
- (30) Spycher, N.; Pruess, K.; Ennis-King, J. CO₂–H₂O mixtures in the geological sequestration of CO₂. I. Assessment and calculation of mutual solubilities from 12 to 100 °C and up to 600 bar. *Geochim. Cosmochim. Acta* **2003**, *6–7*, 3015–3031.
- (31) Chun, B. S.; Wilkinson, G. T. Interfacial tension in high-pressure carbon dioxide mixtures. *Ind. Eng. Chem. Res.* **1995**, *34*, 4371–4377.
- (32) Tewes, F.; Boury, B. Thermodynamic and dynamic interfacial properties of binary carbon dioxide–water systems. *J. Phys. Chem. B* **2004**, *108*, 2405–2412.
- (33) Kvamme, B.; Kuznetsova, T.; Hebach, A.; Oberhof, A.; Lunde, E. Measurements and modelling of interfacial tension for water + carbon dioxide systems at elevated pressures. *Comput. Mater. Sci.* **2007**, *38*, 506–513.
- (34) Gross, J.; Sadowski, G. Perturbed-Chain SAFT: an equation of state based on a perturbation theory of chain molecules. *Ind. Eng. Chem. Res.* **2001**, *40*, 1244–1260.
- (35) Gross, J.; Sadowski, G. Application of the perturbed-chain SAFT equation of state to associating systems. *Ind. Eng. Chem. Res.* **2002**, *41*, 5510–5515.
- (36) Gross, J.; Spuhl, O.; Tumakaka, F.; Sadowski, G. Modeling copolymer systems using the perturbed-chain SAFT equation of state. *Ind. Eng. Chem. Res.* **2003**, *42*, 1266–1274.
- (37) Cheluget, E. L.; Bokis, C. P.; Wardhaugh, L.; Chen, C. C.; Fisher, J. Modeling polyethylene fractionation using the perturbed-chain statistical associating fluid theory equation of state. *Ind. Eng. Chem. Res.* **2002**, *41*, 968–988.
- (38) Von Solms, N.; Michelsen, M. L.; Kontogeorgis, G. M. Computational and physical performance of a modified PC-SAFT equation of state for highly asymmetric and associating mixtures. *Ind. Eng. Chem. Res.* **2003**, *42*, 1098–1105.
- (39) Kouskoumvekaki, I. A.; VonSolms, N.; Michelsen, M. L.; Kontogeorgis, G. M. Application of the perturbed chain SAFT equation of state to complex polymer systems using simplified mixing rules. *Fluid Phase Equilib.* **2004**, *215*, 71–78.
- (40) Becker, F.; Buback, M.; Latz, H.; Sadowski, G.; Tumakaka, F. Cloud-point curves of ethylene-(meth)acrylate copolymers in fluid ethene up to high pressures and temperatures–Experimental study and PC-SAFT modeling. *Fluid Phase Equilib.* **2004**, *215*, 263–282.
- (41) Tumakaka, F.; Sadowski, G. Application of the perturbed-chain SAFT equation of state to polar systems. *Fluid Phase Equilib.* **2004**, *217*, 233–239.
- (42) García-Sánchez, F.; Elíosa-Jiménez, G.; Silva-Oliver, G.; Vázquez-Roman, R. Vapor–liquid equilibria of nitrogen–hydrocarbon systems using the PC-SAFT equation of state. *Fluid Phase Equilib.* **2004**, *217*, 241–253.
- (43) Spuhl, O.; Herzog, S.; Gross, J.; Smirnova, I.; Arlt, W. Reactive phase equilibria in silica aerogel synthesis: Experimental study and prediction of the complex phase behavior using the PC-SAFT equation of state. *Ind. Eng. Chem. Res.* **2004**, *43*, 4457–4464.
- (44) Tumakaka, F.; Gross, J.; Sadowski, G. Thermodynamic modeling of complex systems using PC-SAFT. *Fluid Phase Equilib.* **2005**, *228–229*, 89–98.
- (45) Cismondi, M.; Brignole, E. A.; Møllerup, J. Rescaling of three-parameter equations of state: PC-SAFT and SPHCT. *Polymer* **2005**, *46*, 108–121.

- (46) Cameretti, L. F.; Sadowski, G.; Mollerup, J. M. Modeling of aqueous electrolyte solutions with perturbed chain statistical associated fluid theory. *Ind. Eng. Chem. Res.* **2005**, *44*, 3355–3362.
- (47) Yelash, L.; Muller, M.; Paul, W.; Binder, K. A global investigation of phase equilibria using the perturbed chain statistical-associating-fluid-theory approach. *J. Chem. Phys.* **2005**, *123*, 1–15.
- (48) Fu, D.; Li, X.-S.; Yan, S. M.; Liao, T. Investigation of critical properties and surface tensions for *n*-alkanes by PC-SAFT combined with density gradient theory and renormalization group theory. *Ind. Eng. Chem. Res.* **2006**, *45*, 8199–8206.
- (49) Fu, D. Investigation of surface tensions for pure associating fluids by PC-SAFT combined with density-gradient theory. *Ind. Eng. Chem. Res.* **2007**, *46*, 7378–7383.
- (50) Cahn, J. W.; Hilliard, J. E. Free energy of a nonuniform system. I. Interfacial free energy. *J. Chem. Phys.* **1958**, *28*, 258–267.
- (51) Bongiorno, V.; Davis, H. T. Modified van der Waals theory of fluid interfaces. *Phys. Rev. A* **1975**, *12*, 2213.
- (52) Bongiorno, V.; Scriven, L. E.; Davis, H. T. Molecular theory of fluid interfaces. *J. Colloid Interface Sci.* **1976**, *57*, 462.
- (53) Carey, B. S.; Scriven, L. E.; Davis, H. T. Semiempirical theory of surface tension of pure normal alkanes and alcohols. *AIChE J.* **1978**, *24*, 1076.
- (54) Carey, B. S.; Scriven, L. E.; Davis, H. T. Semiempirical theory of surface tension of binary mixtures. *AIChE J.* **1980**, *26*, 705.
- (55) Sahimi, M.; Davis, H. T.; Scriven, L. E. Thermodynamic modeling of phase and tension behavior of CO₂/hydrocarbon systems. *Soc. Pet. Eng. J.* **1985**, 235.
- (56) Sahimi, M.; Taylor, B. N. Surface tension of binary liquid–vapor mixtures: A comparison of mean-field and scaling theories. *J. Chem. Phys.* **1991**, *95*, 6749–6761.
- (57) Cornelisse, P. M. W.; Peters, C. J.; Arons, J. S. Application of the Peng–Robinson equation of state to calculate interfacial tension and profiles at vapor–liquid interface. *Fluid Phase Equilib.* **1993**, *82*, 119–129.
- (58) Zuo, Y. X.; Stenby, E. H. A linear gradient theory model for calculating interface tension of mixtures. *J. Colloid Interface Sci.* **1996**, *182*, 126–132.
- (59) Cornelisse, P. M. W.; Peters, C. J.; de Swaan Arons, J. Non-classical interfacial tension and fluid phase behaviour. *Fluid Phase Equilib.* **1996**, *117*, 312–319.
- (60) Cornelisse, P. M. W.; Peters, C. J.; de Swaan Arons, J. On the fundamentals of the gradient theory of van der Waals. *J. Chem. Phys.* **1997**, *106*, 9820–9834.
- (61) Cornelisse, P. M. W.; Wijkamp, M.; Peters, C. J.; de Swaan Arons, J. Interfacial tensions of fluid mixtures with polar and associating components. *Fluid Phase Equilib.* **1998**, *150–151*, 633–640.
- (62) Dee, G. T.; Sauer, B. B. The surface tension of polymer liquids. *Adv. Phys.* **1998**, *47*, 161–205.
- (63) Kahl, H.; Enders, S. Calculation of surface properties of pure fluids using density gradient theory and SAFT-EOS. *Fluid Phase Equilib.* **2000**, *172*, 27–42.
- (64) Miqueu, C.; Mendiboure, B.; Graciaa, A.; Lachaise, J. Modelling of the surface tension of pure components with the gradient theory of fluid interfaces: a simple and accurate expression for the influence parameters. *Fluid Phase Equilib.* **2003**, *207*, 225–246.
- (65) Miqueu, C.; Mendiboure, B.; Graciaa, C.; Lachaise, J. Modelling of the surface tension of binary and ternary mixtures with the gradient theory of fluid interfaces. *Fluid Phase Equilib.* **2004**, *218*, 189–203.
- (66) Miqueu, C.; Mendiboure, B.; Graciaa, A.; Lachaise, J. Modeling of the surface tension of multicomponent mixtures with the gradient theory of fluid interfaces. *Ind. Eng. Chem. Res.* **2005**, *44*, 3321–3329.
- (67) Lin, H.; Duan, Y. Y.; Min, Q. Gradient theory modeling of surface tension for pure fluids and binary mixtures. *Fluid Phase Equilib.* **2007**, *254*, 75–90.
- (68) Vargaftik, N. B. *Tables on the Thermo-Physical Properties of Liquids and Gases*; Hemisphere Publishing Corporation: New York, 1975.
- (69) Lemmon, E. W.; McLinden, M. O.; Friend, D. G. Thermophysical Properties of Fluid Systems. In *NIST Chemistry WebBook*; Linstrom, P. J., Mallard, W. G., Eds.; NIST Standard Reference Database No. 69; National Institute of Standards and Technology: Gaithersburg, MD, 2003.
- (70) Jasper, J. J. The surface tension of pure liquid compounds. *J. Phys. Chem. Ref. Data* **1972**, *1*, 841–1009.

Received for review June 18, 2008

Revised manuscript received August 26, 2008

Accepted September 4, 2008

IE800959H